Journal of Cerebral Blood Flow & Metabolism (2015) 35, 1746–1756

www.jcbfm.com

ORIGINAL ARTICLE

Measuring cerebrovascular reactivity: the dynamic response to a step hypercapnic stimulus

Julien Poublanc[1], Adrian P Crawley[1], Olivia Sobczyk[2], Gaspard Montandon[1], Kevin Sam[3], Daniel M Mandell[1], Paul Dufort[1], Lashmikumar Venkatraghavan[4], James Duffin[3,4], David J Mikulis[1,2] and Joseph A Fisher[1,2,3,4]

We define cerebral vascular reactivity (CVR) as the ratio of the change in blood oxygen level-dependent (BOLD) magnetic resonance imaging (MRI) signal (S) to an increase in blood partial pressure of CO_2 (PCO_2): % Δ S/Δ PCO_2 mm Hg. Our aim was to further characterize CVR into dynamic and static components and then study 46 healthy subjects collated into a reference atlas and 20 patients with unilateral carotid artery stenosis. We applied an abrupt boxcar change in PCO_2 and monitored S. We convolved the PCO_2 with a set of first-order exponential functions whose time constant τ was increased in 2-second intervals between 2 and 100 seconds. The τ corresponding to the best fit between S and the convolved PCO_2 was used to score the speed of response. Additionally, the slope of the regression between S and the convolved PCO_2 represents the steady-state CVR (ssCVR). We found that both prolongations of τ and reductions in ssCVR (compared with the reference atlas) were associated with the reductions in CVR on the side of the lesion. τ and ssCVR are respectively the dynamic and static components of measured CVR.

Journal of Cerebral Blood Flow & Metabolism (2015) **35,** 1746–1756; doi:10.1038/jcbfm.2015.114; published online 1 July 2015

Keywords: BOLD signal; carbon dioxide; cerebrovascular reactivity; dynamic response; humans; hypercapnia; time constant

INTRODUCTION

Clinical Assements of Cerebrovascular Reactivity

In asymptomatic patients with cerebrovascular steno-occlusive disease, cerebral blood flow (CBF) is maintained mainly through autoregulation, utilizing compensatory vasodilation.[1] Cerebral blood flow is usually sufficient to maintain normal capabilities such as sensation and movement, but careful surveys reveal subtle reductions in cognitive performance.[2,3] As well, reductions in cerebrovascular reactivity (CVR) have been associated with structural changes such as cortical thinning,[4] white-matter microangiopathic disease,[5] and enhanced risk of stroke.[6,7] These studies suggest that localizing impaired CVR and quantifying its severity would complement neurologic assessment.

Measuring Cerebrovascular Reactivity

Hypercapnia, an increase in the partial pressure of CO_2 in arterial blood ($PaCO_2$), measured in mm Hg, is a well-characterized cerebral vasodilatory stimulus.[8] Assuming no change in oxygen consumption from normocapnia to hypercapnia, the blood oxygen level-dependent magnetic resonance (BOLD MR) signal (S) can be used as a surrogate for change in CBF.[9] The BOLD signal response provides a high spatial and time resolved indication of the direction and magnitude of changes in CBF.[10,11] Cerebrovascular reactivity is here defined and calculated as the per cent change in BOLD signal per change in end-tidal partial pressure of CO_2 ($P_{ET}CO_2$) and expressed as %S/mm Hg.

The speed of Cerebrovascular Reactivity Response

Another assessment of vascular function that may be useful is the *rate* of CBF increase in response to an abrupt vasodilatory stimulus. The time course of middle cerebral artery flow velocity in response to a step hypercapnic stimulus has some variation between healthy subjects.[12,13] CVR also varies within individual subjects between gray and white matter.[14]

Cerebral blood flow vasodilatory response times have also been found to be consistently longer in patients with mild dementia and Alzheimer's disease than in age-matched, healthy subjects.[10,15,16] In the course of a recent study of the amplitude of the BOLD signal response to hypercapnia in patients with cerebrovascular steno-occlusive disease,[17] we also noticed that the time course of signal changes can vary greatly throughout the brain within gray and white matter in healthy subjects, and between healthy subjects and patients, particularly in locations close to those experiencing vascular steal.

A Step Hypercapnia to Measure the Speed of Cerebrovascular Response

The simplest stimulus that is useful for measuring the speed of the CBF vasodilatory response is a step (i.e., square wave) increase in $PaCO_2$. This is not provided by breath holding or even an abrupt change in *inspired* PCO_2.[18] The latter produces a biexponential rise as the CO_2 is first 'washed in' to the lung, gradually rising to an asymptote as CO_2 elimination comes into equilibrium with the

[1]Joint Department of Medical Imaging, University Health Network, Toronto, Ontario, Canada; [2]Institute of Medical Science, University of Toronto, Toronto, Ontario, Canada; [3]Department of Physiology, University of Toronto, Toronto, Ontario, Canada and [4]Department of Anaesthesia and Pain Management, University Health Network, Toronto, Ontario, Canada. Correspondence: J Poublanc, MSc, Joint Department of Medical Imaging, Toronto Western Hospital, University Health Network, McLaughlin Pavilion, 3rd floor, Rm 400, 399 Bathurst Street, Toronto, Ontario M5T 2S8, Canada.
E-mail: julienpoublanc@gmail.com
Financial support from the Canadian Stroke Network and the Ontario Research Fund is gratefully acknowledged.
Received 4 December 2014; revised 13 April 2015; accepted 14 April 2015; published online 1 July 2015

body CO_2 production.[19] With either of these methods $P_{ET}CO_2$ is not a reliable indicator of $PaCO_2$,[20,21] so that neither the time course nor the magnitude of the stimulus is precisely known, and therefore difficult to synchronize with the vascular response.[16] In contrast, sequential gas delivery breathing circuits administer a gas composition supplied by a computerized gas blender, followed by rebreathing of previously exhaled gas. This system enables the implementation of an abrupt (within 1 to 2 breaths) step increase in $P_{ET}CO_2$, which is sustained constant and independent of the pattern or extent of breathing. The rebreathing aspect also reduces the gradient between $P_{ET}CO_2$ and $PaCO_2$. Further details of the system are provided in Materials and Methods section.

Aims of the Study

The aim of the study was to develop a method of separating CVR into (1) a dynamic component providing a voxelwise measurement of the speed of the cerebrovascular response to hypercapnia and (2) a static component providing a measure of the steady-state reactivity of the vasculature. We then applied these analyses to a cohort of patients with known localized cerebrovascular compromise, and compared the findings with those in healthy subjects.

Since our stimulus consisted of an abrupt step change in $PaCO_2$, for our analysis, we assumed a first-order exponential response of the vasculature to the stimulus. We therefore convolved the known input signal with a first-order exponential to identify the $P_{ET}CO_2$ series providing the best fit with the time course of the BOLD signal, voxel by voxel. We used the time constant (τ) of the exponential providing the best fit to score the response dynamics, and the slope of the regression between the BOLD signal and the convolved $P_{ET}CO_2$ to score the steady-state CVR (ssCVR).

We illustrate this method by applying it to 20 patients with known steno-occlusive disease, and 46 healthy control subjects. Our hypothesis was that the speed of response would be abnormally slow predominantly in the hemispheres on the side of the carotid artery stenosis, when compared with that in the corresponding hemispheres of the healthy cohort, and with the contralateral hemisphere in the same patient.

MATERIALS AND METHODS

Subjects and Ethical Approval

These studies conformed to the standards set by the latest revision of the Declaration of Helsinki. They were approved by the Research Ethics Board of the University Health Network and all subjects had given written informed consent. We drew 20 patients from our database,[22] with the following inclusion criteria: the presence of unilateral severe steno-occlusive large vessels disease, abnormalities in CVR, and a normal anatomic scan. Patients could be either sex, and any age. Patient files were selected before any data analysis, and none were rejected after analysis. In addition, we analyzed test data obtained from 46 healthy volunteers who had undergone the same stimulus and scanning protocol as the patients. The anthropomorphic characteristics and CVR findings for these subjects have been reported elsewhere.[23]

Experimental Protocol

Hypercapnic stimulus. All subjects and patients were asked not to engage in heavy exercise or drink caffeinated drinks on the day of the test. Control of $P_{ET}CO_2$ and the end-tidal partial pressure of oxygen were implemented with a computer-controlled gas blender (RespirAct, Thornhill Research Inc., Toronto, ON, Canada).

The standardized sequence of $P_{ET}CO_2$ changes is presented in Figure 1. After 60 seconds at a baseline $P_{ET}CO_2$ of 40 mm Hg, $P_{ET}CO_2$ was increased over one or two breaths to 50 mm Hg for 45 seconds, followed by a return to baseline for 90 seconds; a second step hypercapnia was sustained for 120 seconds followed again by return to baseline for 60 seconds. End-tidal PO_2 was maintained constant at 100 mm Hg throughout testing. The system is implemented using an automated gas blender running a prospective targeting algorithm.[24] $P_{ET}CO_2$ transitions were achieved within two breaths and $P_{ET}CO_2$ was maintained constant within 2 mm Hg thereafter.[8] For the healthy cohort, the mean and standard deviation increase in $P_{ET}CO_2$ was 9.2 ± 0.7 mm Hg.

The mechanism of gas control and the rationale for its use is described elsewhere.[8,24] In brief, a volume and concentration of CO_2 required to increase the $P_{ET}CO_2$ by a targeted amount, say, 10 mm Hg, is administered at the beginning of the breath, followed by rebreathed gas which displaces the initial gas bolus of CO_2 into the alveoli and thereby determines alveolar gas exchange and the $P_{ET}CO_2$. The rebreathed gas had already equilibrated with capillary blood so it has no further effect on CO_2 exchange, enabling the gas exchange to be independent of ventilation. The end-inspiratory rebreathing also narrows the gradient between $P_{ET}CO_2$ and $PaCO_2$, resulting in $P_{ET}CO_2$ being practically equal to the $PaCO_2$.[25,26] For clarity, we will hereafter refer to the stimulus as $P_{ET}CO_2$ when referring to what is measured, and $PaCO_2$ when referring to the actual physiologic stimulus. Ours is the first study in which the course of the actual stimulus, the $PaCO_2$, was convolved with the output signal, in this case, BOLD.

Magnetic resonance imaging protocol. Magnetic resonance imaging was performed with a 3.0-Tesla HDx scanner using an 8-channel phased-array receiver coil (Signa; GE Healthcare, Milwaukee, WI, USA).

Cerebrovascular reactivity images were acquired using a BOLD MR pulse sequence with the following parameters: echo planar imaging gradient echo with repetition time/echo time = 2,000/30 ms, $3.75 \times 3.75 \times 5$ mm voxels, field of view 24×24 cm, 39 slices, slice thickness 5 mm, matrix size 64×64, number of frames = 254, flip angle = 85°. T1-weighted images were acquired for coregistration and spatial normalization purposes. An inversion recovery-prepared spoiled gradient-recalled sequence was used with the following parameters: flip angle = 20°, inversion time/echo time/repetition time = 300/5/11.5 ms, 146 slices of 1 mm thickness and a 256×256 matrix size with 200 mm field of view.

Data Processing

Initial analysis. The acquired BOLD MRI and $P_{ET}CO_2$ data were transferred to an independent workstation and analyzed using AFNI software,[24] Matlab 8.1/R2013a (http://www.mathworks.com/products/matlab) and SPM5 (http://www.fil.ion.ucl.ac.uk/spm). Slice-time correction, followed by volume re-registration for motion correction during scanning, was applied to the raw data set.

Cerebrovascular reactivity maps. The recorded $P_{ET}CO_2$ stimulus was time shifted to the point of maximum correlation with the whole brain average BOLD signal. Cerebrovascular reactivity was then calculated as a linear, least-squares fit of the BOLD response (S) to the $P_{ET}CO_2$ stimulus on a voxel-by-voxel basis (Figure 2). In other words, S was fitted using the following equation:

$$S(t) = CVR \times P_{ET}CO_2(t) + B + \varepsilon(t) \quad (1)$$

where B is the baseline signal, $\varepsilon(t)$ is the residual time series, and CVR is the slope of the line of regression between $P_{ET}CO_2$ and S, and interpreted as the mean signal change per mm Hg $P_{ET}CO_2$. The CVR for each voxel is color-coded (see Supplementary Table 1) and superimposed on the corresponding voxel of the anatomic scan to generate a CVR map.

τ and steady-state cerebrovascular reactivity maps. We parsed the CVR into a steady-state component (ssCVR) and a dynamic component (τ). The principles of measuring these parameters are outlined schematically in Figures 1 and 2. The BOLD response to a stimulus was modeled as the $P_{ET}CO_2$ convolved with a hemodynamic response functions (HRFs) of the vessels consisting of an exponential decay function of the form: $\exp(-t/\tau)$, where t is the time variable and τ the time constant of response.

$$S(t) = \text{ssCVR} \times \{P_{ET}CO_2(t) \otimes \text{HRF}(t, \tau)\} + B + \varepsilon(t) \quad (2)$$

Note that the operation substitutes the independent variable $P_{ET}CO_2(t)$ as used classically in CVR maps, with $P_{ET}CO_2(t) \otimes \text{HRF}(t, \tau)$, with $\text{HRF}(t, \tau) = \frac{e^{-t/\tau}}{C}$ for $0 \leqslant t \leqslant 5 \times \tau$, and normalization constant (area under the curve) $C = \int_0^{5\times\tau} e^{-t/\tau} dt$ and $\text{HRF}(t, \tau) = 0$ for $t > 5 \times \tau$, where the exponential function in the HRF is small enough to be considered null at $t > 5 \times \tau$.

Steady-state CVR is calculated by taking the slope of the regression between the convolved $P_{ET}CO_2$ and S and can be thought of as the CVR corrected for the speed of the response (τ). In other words, ssCVR represents the time-independent response, with the same units as CVR (% S/mm Hg). Figure 2 illustrates the difference between the traditional measure of CVR and ssCVR and how those differences can affect the reactivity measurements as well as the goodness of the fit.

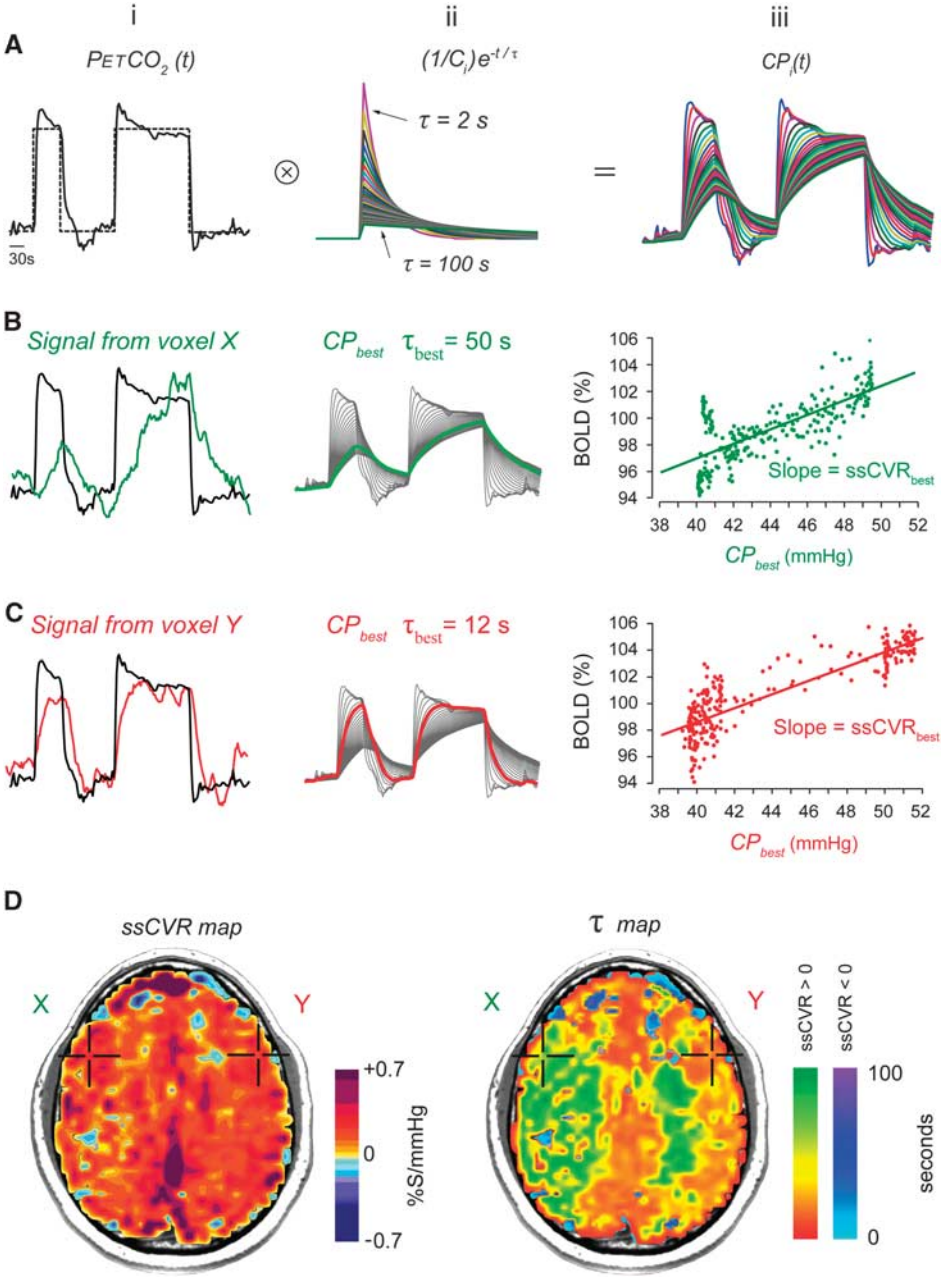

Figure 1. Generation of steady-state cerebrovascular reactivity (ssCVR) and time constant (τ) maps from a standardized abrupt two-step stimulus. (**A**) (i) Target (dotted line) and actual (solid line) end-tidal partial pressure of CO_2 ($P_{ET}CO_2$). (ii) The set of first-order exponentials with τ ranging from 2 to 100 seconds used to convolve the actual $P_{ET}CO_2$ to generate a set of convolved curves seen in (iii). (**B** and **C**) (i) Actual $P_{ET}CO_2$ (solid black line) and blood oxygen level-dependent (BOLD) signal (green and red lines) from voxels X and Y, respectively, shown in (**D**). (ii) Set of curves resulting from the convolution of $P_{ET}CO_2$. The highlighted line is that which has the best fit to the voxel BOLD signal shown in (i). (iii) The regression with the best fit between the convolved $P_{ET}CO_2$ and the BOLD signal is shown. The difference in the pattern of the data results from the extent of distortion the convolution imposes on the $P_{ET}CO_2$ input function. (**D**) The ssCVR map is generated from the slope of the line with the highest correlation coefficient as illustrated in the graphs in row (iii). The τ map is generated from the τ of the exponential used to generate the line with the highest correlation coefficient. The ssCVR and the τ values are color coded according to the color scales shown and mapped onto the corresponding voxels in the anatomic scan.

Equation (2) describes the generation of a set of multiple convolved $P_{ET}CO_2$ (CP_i) for τ ranging from 2 to 100 seconds, in 2-second increments (Figure 1A):

$$CP_i(t) = P_{ET}CO_2(t) \otimes \frac{e^{-t/\tau_i}}{C_i}$$

where $i = (1, 2, \ldots, 50)$ and $\tau_i = 2 \times i s$.

A Pearson correlation coefficient is then calculated between S and each of the 50 $CP_i(t)$. The maximal correlation coefficient corresponds to the $CP_i(t)$ that best fit the BOLD signal (CP_{best}) (Figures 1Bii and Cii). Its associated time constant (τ_{best}) is recorded and the slope of the regression ($ssCVR_{best}$) between the BOLD signal and CP_{best} is calculated (Figures 1Biii and Ciii). This process is repeated for each voxel, color coded (Supplementary Table 1), and applied to the corresponding voxels of T_1 maps of the brain to generate maps of ssCVR and τ (Figure 1D).

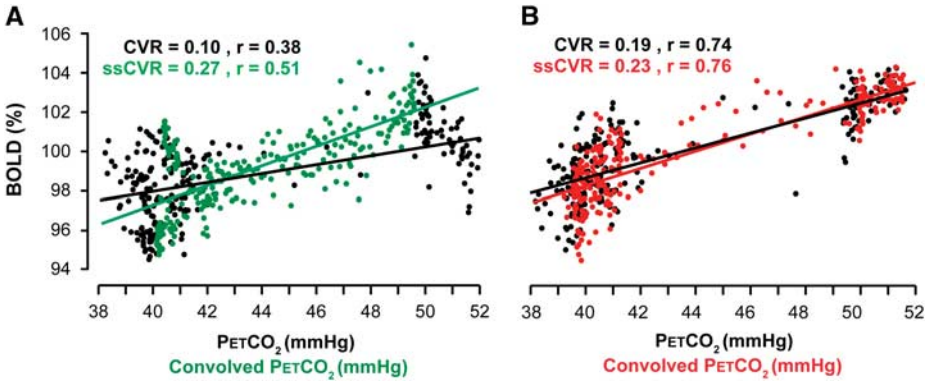

Figure 2. The relationship between cerebrovascular reactivity (CVR) and steady-state CVR (ssCVR). Data from the same patient as presented in Figures 1 and 5. CVR and ssCVR values are expressed in %S/mm Hg. (**A**) Plot of blood oxygen level-dependent (BOLD) signal versus convolved end-tidal partial pressure of CO_2 ($P_{ET}CO_2$) and line of best fit (green dots and line, same data as Figure 1); and the signal versus actual $P_{ET}CO_2$ with its line of best fit (black dots and line), both from the same voxel with slow response. (**B**) Similar graph of signal versus convolved $P_{ET}CO_2$ (red dots and line, same data as Figure 1) and signal versus actual $P_{ET}CO_2$ (black dots and line). Note that when the time course of response is rapid, little convolution of $P_{ET}CO_2$ is required and the CVR is close to ssCVR.

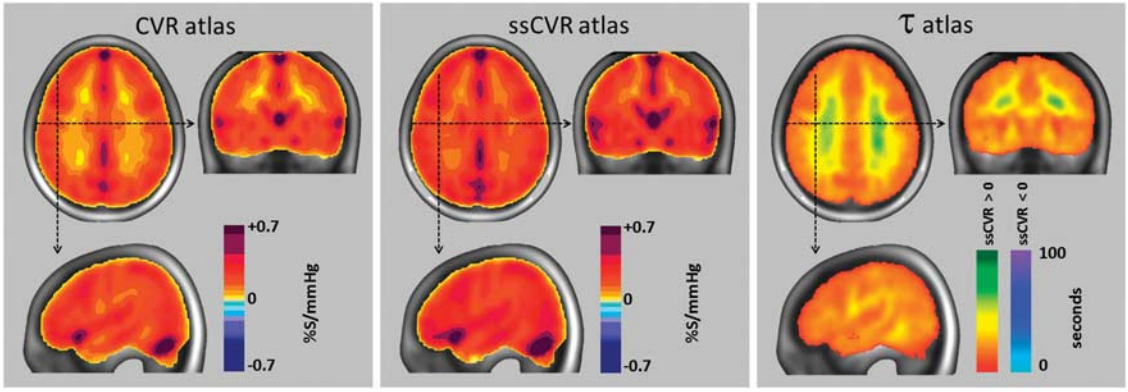

Figure 3. Atlas for cerebrovascular reactivity (CVR), steady-state CVR (ssCVR), and τ from 46 healthy subjects. In each view, the mean value for all corresponding voxels of the atlas was calculated and mapped onto the anatomic image of the standard space using the color scales shown (see Supplementary Table 1 for more detail characterization of the color scales). Areas containing major veins and venous sinuses register greater CVR values due to a reduction in deoxyhemoglobin, and possibly also in diameter, resulting from the reduced extraction fraction, and increased arterial blood volume, respectively, accompanying the hypercapnia-induced increased cerebral blood flow.

z Maps

The data forming our normal atlases were previously reported by Sobczyk *et al*.[25] In that study, these data were used to generate a reference atlas for CVR. For this study, the data were reanalyzed to generate an atlas for each of τ and ssCVR. All scans were re-registered to the T1 MNI template (MNI152) via a nonlinear transformation[27] and spatially smoothed with a full width at half maximum of 5 mm, to minimize intersubject coregistration errors, and merged to form the CVR, ssCVR, and τ atlases (Figure 3). The τ and ssCVR mean (μ) and standard deviation (σ) were calculated for each voxel in the atlas and the respective *z* scores (*z*-ssCVR and *z*-τ) were then calculated for each voxel in the patient scan in a manner analogous to *z*-CVR scores;[23] as follows:

$$z-\mathrm{ssCVR}=\frac{\mathrm{ssCVR}_p-\mu_{\mathrm{ssCVR}}}{\sigma_{\mathrm{ssCVR}}}$$

$$z-\tau=\frac{\tau_p-\mu_\tau}{\sigma_\tau}$$

Subscript p refers to patient's value and μ and σ to the atlas voxel mean and standard deviation respectively over the 46 healthy subjects.

RESULTS

Figure 3 is a graphical representation of the atlas mean values of CVR, ssCVR, and τ. Summary data from all patients are provided in Figures 4 and 5 with representative axial slices displaying CVR, *z*-CVR, and *z*-τ from each patient. Table 1 presents a sketch of their clinical information. Three examples were chosen to illustrate the results in greater detail. One example healthy subject was randomly chosen from the reference cohort (Figure 6), and two representative patients were chosen to show 'moderate' (Figure 7; patient 20, Figure 5) and 'severe' (Figure 8 and patient 10, Figure 4) disease.

In all patients, the BOLD signal achieved a better fit to the convolved $P_{ET}CO_2$ than to the actual $P_{ET}CO_2$. Figure 2 shows the goodness of fit of the BOLD signal to actual $P_{ET}CO_2$ and to convolved $P_{ET}CO_2$ in a healthy and compromised voxel. In the same patient ('Moderate'), the average R^2 for the BOLD signal versus convolved $P_{ET}CO_2$ was greater than for the BOLD versus actual $P_{ET}CO_2$ in both hemispheres: 0.19 versus 0.13 ipsilateral to the stenotic lesion, and 0.41 versus 0.37 in the contralateral hemisphere. The magnitude of the discrepancies in the R^2 indicates the extent to which speed of response contributes to

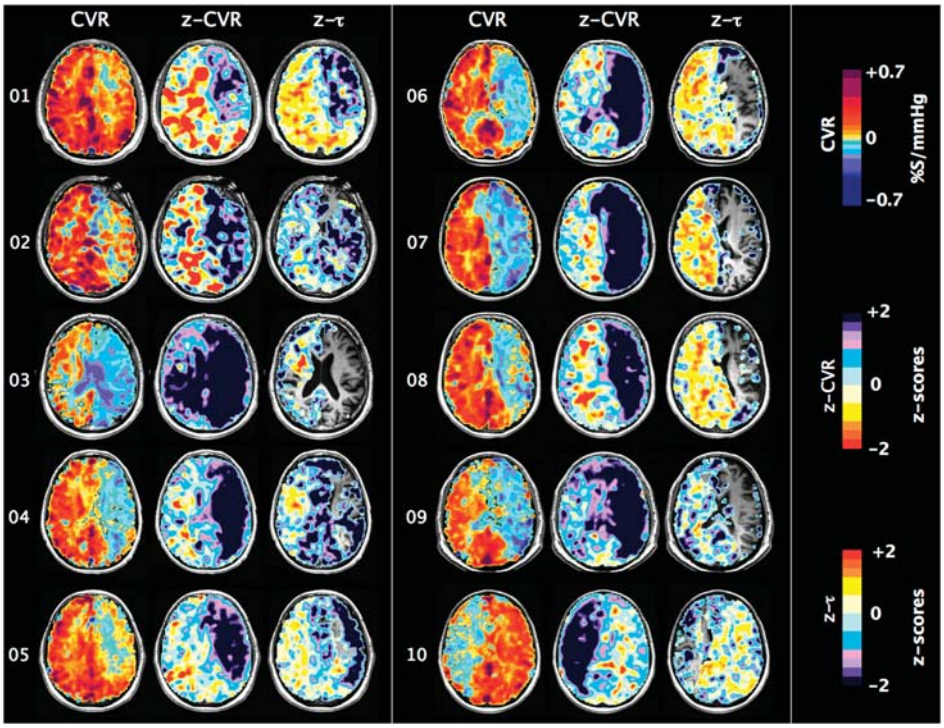

Figure 4. One slice of CVR, z-CVR and z-τ maps for patients number 01 to 10. Patients' characteristics are presented in Table 1.

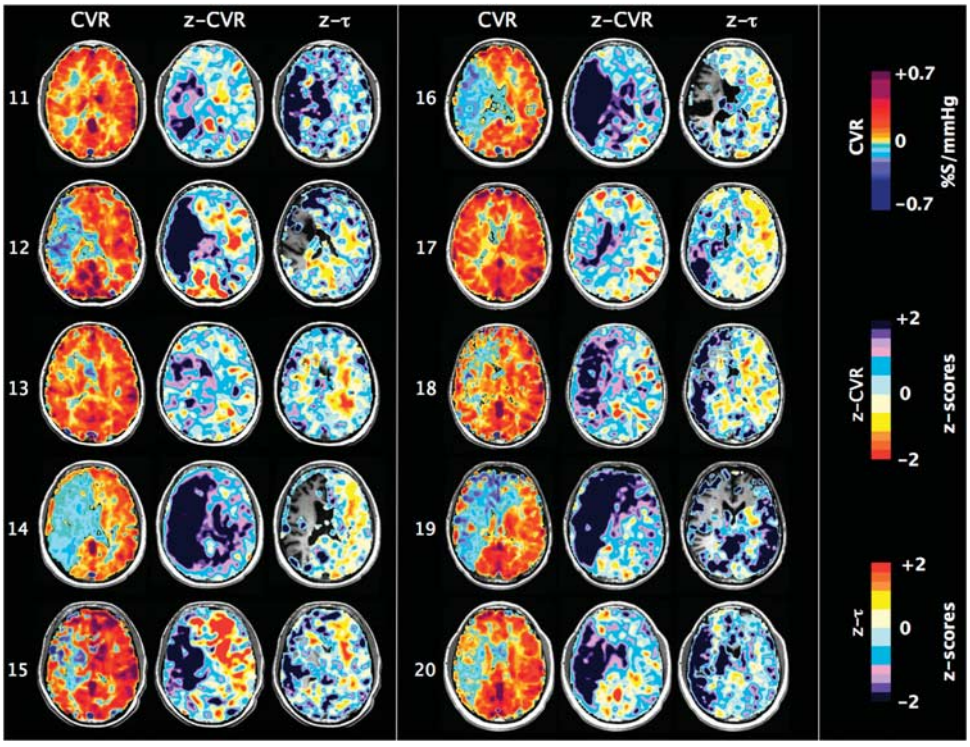

Figure 5. One slice of CVR, z-CVR and z-τ maps for patients number 11 to 20. Patients' characteristics are presented in Table 1.

the measured CVR, and in pathologic areas, to regional vascular dysfunction.

Examination of the maps in Figures 6–8 shows that, in general, CVR and ssCVR are smaller, and τ much longer in deep white matter compared with gray matter. All 20 patients showed some degree of 'steal' (i.e., reduction in flow from baseline in response to a hypercapnic stimulus) in the hemisphere supplied by the occluded artery; steal occurred predominantly in subcortical white

Table 1. Patient Characteristics

Case No.	*Age, Years*	*Sex*	*Side of Steno-occlusive Disease*	*Angiographic Findings, Affected hemisphere*	*Angiographic Findings, Unaffected Hemisphere*
01	53	M	L	High-grade supraclinoid ICA stenosis	No abnormality
02	63	M	L	ICA occlusion at carotid siphon	No abnormality
03	83	M	L	Occlusion of supraclinoid ICA, hypoplastic P1, large left pcom	No abnormality
04	75	M	L	Proximal ICA occlusion near bifurcation	Hypoplastic right vertebral
05	55	M	L	High-grade petrous ICA stenosis, small cavernous portion, narrow M1 segment, narrow A1 segment	No abnormality
06	63	M	L	ICA occlusion at carotid siphon	No abnormality
07	54	F	L	ICA occlusion at carotid siphon	No abnormality
08	67	F	L	ICA occlusion at supraclinoid segment	No abnormality
09	74	M	L	ICA occlusion at carotid siphon	No abnormality
10	59	M	R	Distal ICA occlusion	No abnormality
11	35	M	R	High-grade cervical ICA stenosis, hypoplastic M1 segment	No abnormality
12	60	M	R	ICA occlusion at origin	30% cavernous ICA stenosis
13	70	M	R	ICA occlusion at carotid siphon	No abnormality
14	85	M	R	ICA occlusion at carotid bifurcation in neck	No abnormality
15	67	M	R	High-grade ICA stenosis at carotid siphon, hypoplastic M1 segment	No abnormality
16	62	F	R	Supraclinoid ICA occlusion	No abnormality
17	25	M	R	High-grade ICA stenosis near termination, narrow A1 and M1 segments	No abnormality
18	79	M	R	High-grade stenosis near carotid bifurcation in neck	Mild stenosis in proximal extracranial ICA
19	56	M	R	ICA occlusion at cervical segment	Mild ICA stenosis after carotid bifurcation
20	46	M	R	ICA occlusion	No abnormality

F, female; ICA, internal carotid artery; L, left; M, male; PCA, posterior cerebral artery; R, right.

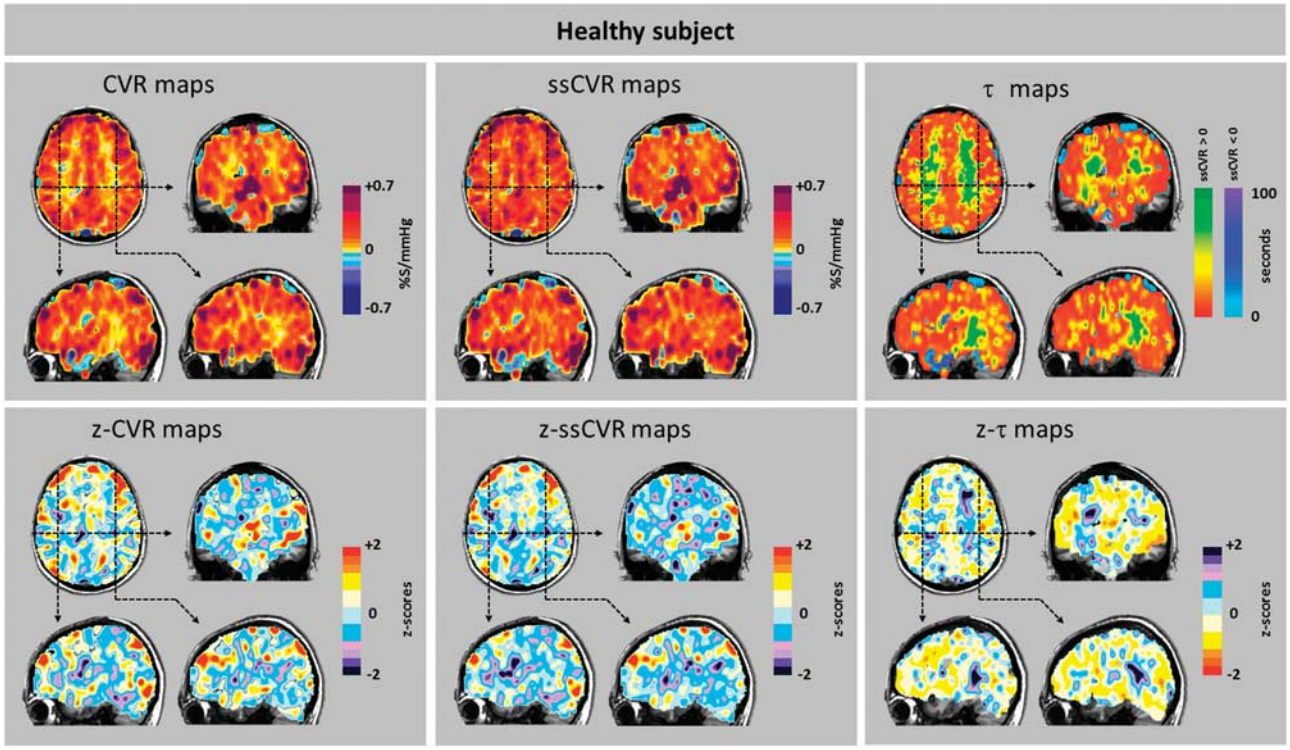

Figure 6. Cerebrovascular reactivity (CVR), steady-state CVR (ssCVR), τ, and respective z maps from a healthy patient. Top row: The CVR map reflects the net response of both the amplitude signal and its time course seen in isolated form in the ssCVR map and τ map, respectively. Bottom row: The z maps illustrate the extent and distribution of z values in a healthy subject. The yellow tinge to the z-τ map indicates briskly responding vasculature within the normal range.

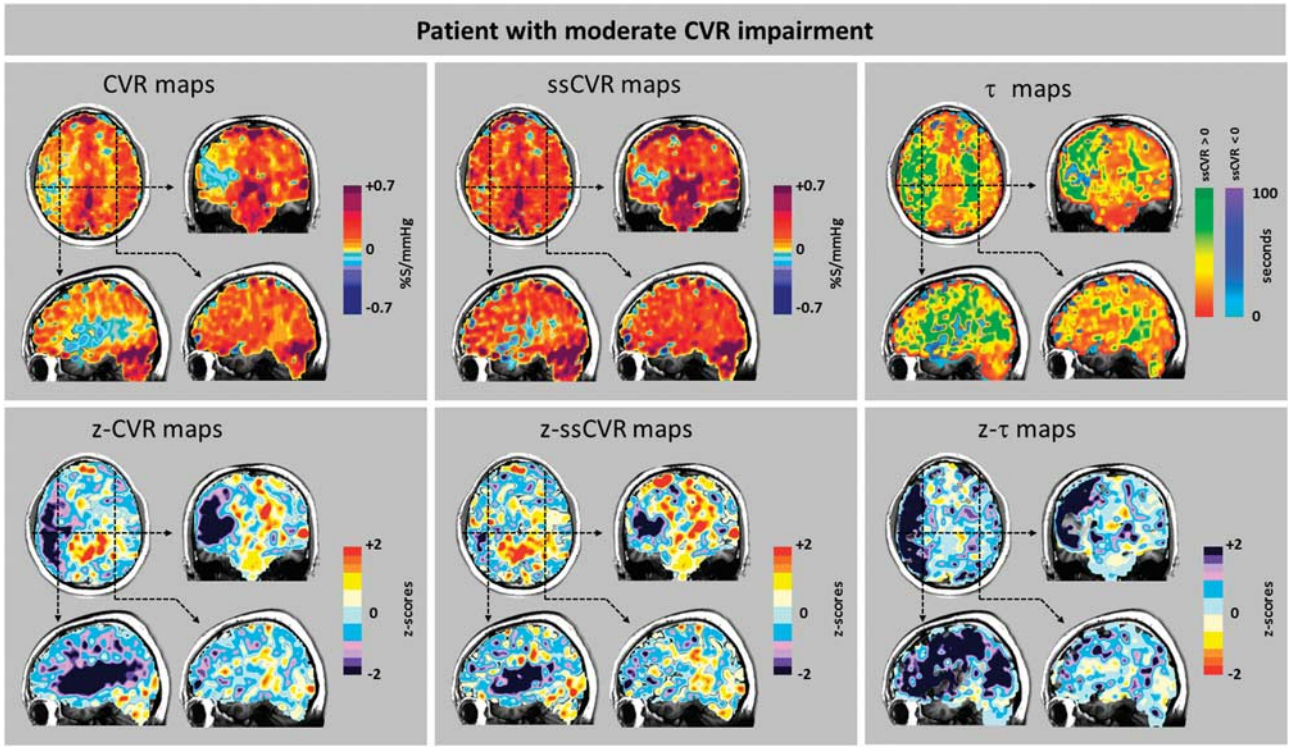

Figure 7. Cerebrovascular reactivity (CVR), steady-state CVR (ssCVR), τ, and respective *z* maps from a patient (patient 20, Figure 5) showing moderate changes. Scans from a 46-year-old male with a history of hypertension, type II diabetes mellitus, and hypercholesterolemia who presented to hospital with transient symptoms of slurred speech, dizziness and memory loss, left facial droop, and left side weakness. Magnetic resonace angiography showed right carotid artery occlusion, and anatomic magnetic resonance imaging scans were normal. Top row: The CVR map shows steal in the cortical area. ssCVR maps show a smaller extent of changes, suggesting that the CVR changes strongly affected by changes in time of response. Bottom row: The *z*-CVR maps show that the reductions in amplitude of response are primarily in the right cortical territory. In the cortical gray matter, the *z*-τ map shows that the spatial extent of reduced rate of vascular response is much more extensive than the extend of the reduced reactivity in the *z*-CVR.

matter. The *z*-CVR maps indicate that the outer rim of the steal areas has reduced CVR compared with normal. The *z*-τ maps show abnormally prolonged τ in areas of positive CVR contiguous to, or surrounding, areas of steal.

Whereas there were prolonged τ in voxels in white matter and some gray matter areas which retained positive CVR, there were, remarkably, reduced τ in the areas with negative CVR. Indeed, τ was shortest in the areas where the reduction in CVR and *z*-CVR—i.e., steal—was the greatest, as has previously been reported.[28] The explanation for these observations is that the greatest degree of steal during hypercapnia occurs in the vessels that have lost the most vascular tone; they respond passively and therefore their response profiles are the mirror image of those in vascular beds capable of brisk increases in flow. Sobczyk *et al*[17] have verified the passive responses of these vessels by demonstrating paradoxical *increases* in flow in areas of steal ('reverse steal'), which accompanies a global vasoconstrictive stimulus. Thus, whereas short τ in areas of positive CVR reflects robust responses, short τ in areas of negative CVR reflects the opposite: the loss of vascular reactivity. As such, τ values in areas with negative CVR are not on the same continuum of severity of disease as those from positive CVR and cannot be scored by reference to the same atlas. We therefore did not generate *z*-τ scores for the areas with negative CVR in Figures 6–8 and Figure 4.

In some patients (Figures 4 and 5, patients 1, 2, 4–8, 12, 15), the hemisphere contralateral to that with the carotid artery stenosis showed extensive areas with unusually increased CVR compared with normal. In some of these (patients 1, 5–8), τ was also unusually short compared with normal. However, among those patients where there was a poor CVR response in the contralateral hemisphere, some (1, 5–7, 10, 13, 17, 18) nevertheless had short τ.

Values for ssCVR were generally greater than for CVR, particularly when τ is long. This finding is a consequence of CVR reflecting both the magnitude and the speed of response to a stimulus as illustrated in Figure 2. In the 'moderate' patient (Figure 7) CVR was positive but diminished, corresponding to the abnormally long τ values in gray matter of the right hemisphere ipsilateral to the carotid occlusion. However, in the patient with 'severe' changes (Figure 8), in addition to the low CVR, long τ and positive ssCVR voxels, there were voxels where ssCVR and CVR are negative, i.e., there is vascular steal.[17] In the latter case, as discussed above, no *z*-τ data are provided.

DISCUSSION

Main Findings

In this study, we describe a method to calculate the speed of response to a hypercapnic stimulus, designated by the time constant τ of a fit first-order exponential, and the time-independent magnitude of change of the BOLD response, named ssCVR, to a step vasoactive stimulus. The application of the method was illustrated in 20 patients with unilateral steno-occlusive large cerebral vessel disease. There were various patterns of coherence and discordance of CVR, ssCVR and τ in both the ipsilateral and contralateral hemispheres. It is therefore apparent that they do not measure exactly the same parameter of vascular physiology. We found that τ was characteristically prolonged in areas

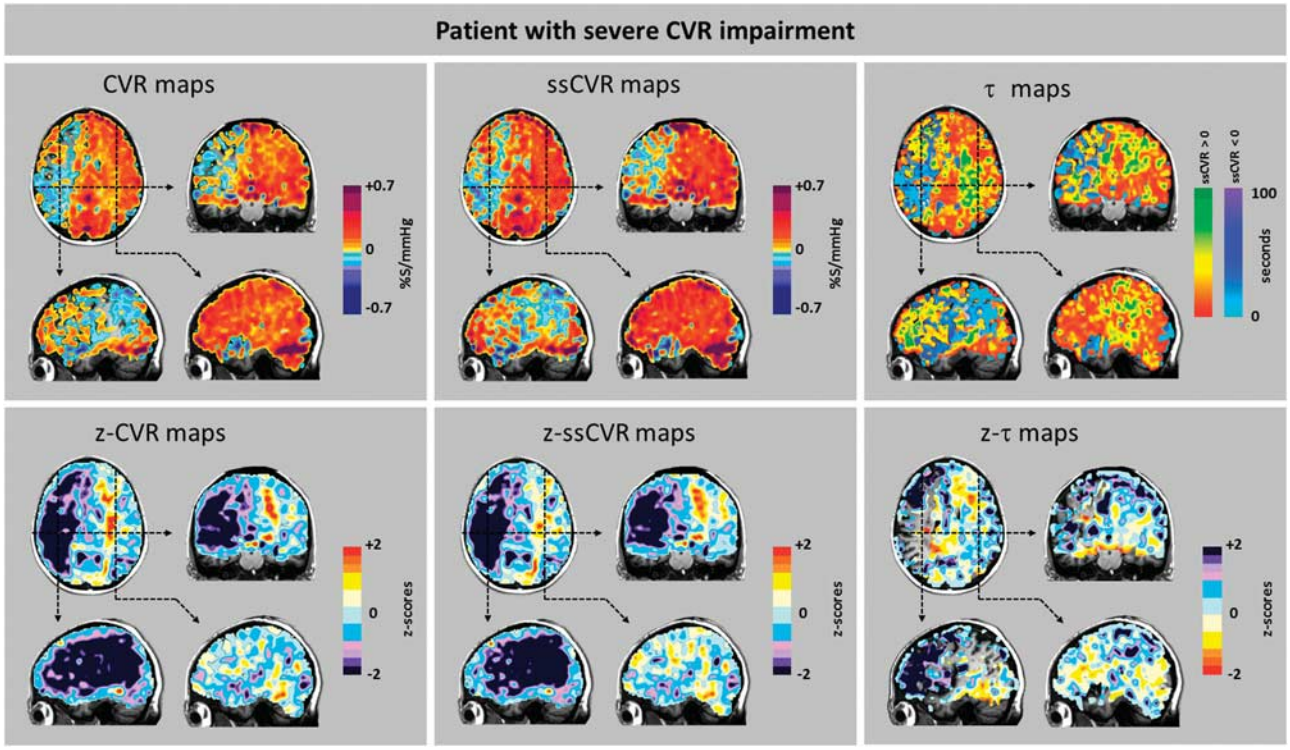

Figure 8. Cerebrovascular reactivity (CVR), steady-state CVR (ssCVR), τ, and respective z maps from a patient (patient 10, Figure 4) showing severe changes. Scans from a 58-year-old male with a history of treated hypertension and lymphoma who presented for investigation of a new onset of recurrent transient left sided weakness. There were no neurologic deficits on clinical examination. Imaging showed that the right internal carotid artery was occluded above the origin by a calcified plaque. The left system was free of disease. The anterior and posterior communicating arteries were patent. Top row: CVR and ssCVR maps are nearly identical indicating the predominance of reductions in CVR over reductions in τ. The τ map requires different interpretations regarding the severity of underlying pathology in the areas with positive response (red-green color scale) and those with negative response (blue color scale). This is discussed in greater detail in Results section. Bottom row: The z maps show that reduced CVR is mostly due to reduced amplitude of response. Note that the z-τ map shows only voxels with positive τ.

downstream from high-grade carotid stenosis while it remained closer to the normal range in the contralateral hemisphere.

τ as an Indicator of Abnormal Cerebrovascular Response

Cerebral vascular reactivity is, by definition, dynamic and it is appropriate to seek to characterize its speed of response. To examine the relationship between CVR and τ, we deliberately chose patients with known unilateral cerebrovascular disease, normal structural MRI scans, and abnormal vascular responses in the form of abnormal CVR. We considered that the presence of unilateral disease and abnormal CVR would allow comparisons of τ in areas of known vascular compromise (ipsilateral to the carotid artery occlusion), to the normal vasculature of the contralateral hemisphere in the same subject.[11] Indeed, in our patients, the distribution of severely abnormal CVR and τ was consistent with the location of the lesion shown by angiography in all 20 subjects. We suggest that the large contiguous swaths of abnormal voxels of CVR and τ consistent with each other and with angiographic findings are highly unlikely to occur by chance and more likely to result from common underlying vascular pathology.

While reductions in CVR have long been suspected to occur in dementia, reductions in the rate of vascular response have now been shown to be the strong markers of the disease.[16,29] Since our method of comparison to an atlas appears to have been sufficiently sensitive to identify abnormal reductions in CVR and lengthening of τ in individual patients with steno-occlusive vascular disease, we suggest that this method may confer the same advantages in assessing patients with dementia.

Universally Accessible Data: *z* Scoring Relative to a Site-Specific Reference Cohort

This study, as that by Sobczyk *et al*,[23] follows the convention of reporting its data in the form of z scores with reference to a site-specific atlas to make the data compatible with, and accessible to, other investigators.

Normalizing data relative to a reference atlas was introduced by Minoshima *et al*[30] and Chetelat *et al*.[31] These investigators used the method to compare the magnitude of effects of two different parameters (cerebral atrophy measured with MRI and glucose metabolism measured by positron emission tomography) in the same anatomic locations in the brain. They reduced the respective measures to the same units: z scores relative to the means of a reference atlas. Since our study used the same stimulus, MRI scanner, and scanning sequences, we reanalyzed the CVR atlas database of Sobczyk *et al*[23] to generate the atlas for ssCVR and τ. As in the previous report on z maps of CVR,[23] we found that the z maps of ssCVR and τ enhanced the assessment of pathophysiology.

Rather than thresholding voxels of CVR, ssCVR, and τ, we provide the range of their respective z scores. This approach informs on the likelihood of any voxel belonging to the normal range. For any single voxel, we consider that $z > |2|$ to be highly abnormal. The same approach can be used to score the normality of any region of interest (ROI). The average of the z sores in an ROI in the cohort of healthy subjects is expected to be $0 \pm$ the standard error of the mean (SEM) z ROI z scores. An abnormal average z score for CVR, ssCVR, or τ in an ROI would be defined as having a mean z score in the corresponding ROI $> |2|$ SEM.

The Importance of a Standard Stimulus

All methods of quantifying the time constants of response require the fitting of a response signal to an input signal. In previous studies, the input signals were inexact, consisting of timing 'on/off' for the presence or absence of inspired CO_2,[16,29] or used the $P_{ET}CO_2$ as an inexact surrogate for the $PaCO_2$.[14,15] Furthermore, administering the CO_2 stimulus by changing the *inspired* CO_2 concentration is problematic. Even if performed abruptly, the CO_2 lung concentration, and hence the $PaCO_2$, rises more gradually following a wash-out kinetics pattern with a time constant of about 30 seconds.[32]

Our system of administering the stimulus conveyed three novel and advantageous features to the study. First, the targeting system provided a consistent stimulus to all subjects and patients. The standardized stimulus substantially reduced the subject to subject variability in CVR, enabling the generation of an atlas from the healthy cohort and comparison of the patients with the atlas. Second, the end-inspiratory rebreathing feature of the system equalizes the $P_{ET}CO_2$ with the $PaCO_2$ enabling noninvasive breath by breath access the true input signal. Finally, the system applied a rapid step change input signal. Although the time course of signal change is affected by both the rate of change of PCO_2 in the lung, and that of the vessels, in our study, the rate of change in lung PCO_2, and hence in the arterial blood, was a true step; the observed τ can therefore be attributed predominantly to the speed of response of vessels.

Application of Cerebrovascular Reactivity and its Dynamic Parameter to Other Neurovascular Disease

The findings in our cohort are explained by our model[17] of steno-occlusive disease causing widespread downstream loss of vasodilatory reserve, resulting in steal, and abnormal τ and ssCVR in remaining areas with positive CVR. However, vasodilatory reserve can be lost in other ways such as through infectious disease, particularly those related to herpes zoster,[33] noninfectious inflammatory conditions,[34] drug reactions,[35] neoplastic changes,[36] dementia,[29] and traumatic brain injury.[37] We anticipate that studies of τ in these conditions may further elucidate the vascular component of their underlying pathophysiology.

Limitations

In comparison with anatomic and structural imaging, these functional tests have a unique set of challenges. They cannot be validated with independent measures such as angiography or consistency with clinical history or physical signs on examination. Cerebrovascular reactivity, ssCVR, and τ are indirect measures of vascular function; however, they are not fundamentally different from other well-established functional measures of vascular reactivity in other vascular beds such as brachial artery hyperemia in the arm and uptake of radionucleotides to measure changes in myocardial blood flow in cardiac stress testing.

While the assumption of a single exponential response for the dispersion function is reasonable for a preliminary study, a more rigorous study of the nature of the response may show other relationships, including a biexponential response.

For the *z*-tau maps we made the assumption that τ is normally distributed in healthy subjects. We applied the Anderson–Darling test (the statistical test for normality) provided in AFNI (National Institutes of Health) and found most voxels distributed widely throughout the brain scans had attained P values > 0.05 and were assumed to pass the test. The simplifying assumption was therefore made that the τ for each voxel was normally distributed among healthy subjects. We also recognize that the change in τ may not be linearly related to the extent of pathology. This aspect is not addressed by the *z* map approach. The *z* map approach for τ can provide at best only a rank scoring of abnormality.

Our subjects were selected for criteria of unilateral disease, normal anatomic scan, and abnormal CVR study and thus are not necessarily representative of all patients with extracranial large vessel disease. Our reference atlas was nonspecific with respect to age, sex, co-morbidities, medication, and other issues. We also did not select our patient cohort for these characteristics. The large intersubject variability in CVR and τ reduces the sensitivity of detection of abnormalities, but conversely increases specificity. It is nevertheless remarkable that we were able to identify pathologic τ in the ipsilateral hemisphere, and normal τ in the contralateral hemisphere in all 20 subjects.

There are a number of considerations with the use of the BOLD signal as a surrogate for CBF in the convolution of the actual $P_{ET}CO_2$. The BOLD signal does increase with CBF, but it does so as a result of the dilution of the concentration of deoxyhemoglobin ([dHb]) with oxyhemoglobin as the oxygen extraction fraction decreases, consequently veering from a linear relationship at very high, and very low flows.[38,39] A second consideration is the increase of BOLD signal that accompanies the increase in cerebral blood volume (CBV) resulting from hypercapnia. A third consideration is the effect of changes in $PaCO_2$ on cerebral metabolic rate. A fourth issue is that the relationship between change in BOLD and change in $PaCO_2$ is strongly dependent on the baseline $PaCO_2$.[10,40] Finally, changes in PaO_2 during changes in $P_{ET}CO_2$ also affect the BOLD signal.[41,42] We address each of these issues in turn.

In this study, BOLD provided a practical surrogate measure for CBF. The sequences to generate the BOLD signal are widely available in clinical magnets. Assuming a linear CBF response to PCO_2 over the $PaCO_2$ range of our study,[43] the Davis [dHb] dilution model would predict a fairly linear range of resulting BOLD signal. Indeed, the BOLD signal was strongly correlated with simultaneously measured brain oxygenation using near infrared spectroscopy during hypercapnic stimulation.[44] In normal subjects, the fractional change in baseline $CBV/CBV_0 = (CBF/CBF_0)^{\propto}$ where $\propto \approx 0.29$ indicates that its contribution to BOLD is small compared with that of CBF. In the absence of consistent evidence to the contrary, it is also widely assumed that the 10 mm Hg hypercapnic stimulus has not affected the cerebral metabolic rate (see Yezhuvath *et al*[45] and Yablonskiy[46] for discussion). The strong dependence of the CVR—regardless whether it is measured by BOLD or arterial spin labeling (ASL)[40]—on the baseline $PaCO_2$ was mitigated by initializing all subjects' $PaCO_2$ to baseline values. Finally, the effect of PaO_2 was mitigated by maintaining normoxic isoxia during hypercapnia.

Although a true measure of CBF such as ASL would be preferred for measuring CVR, there are issues with current implementations of ASL such as spin tag delay sensitivity that increases with increasing severity of vascular disease rendering CBF measurement less accurate. Halani *et al*[40] have presented a cogent deliberation comparing the advantages and limitations of BOLD and ASL for use as surrogate CBF measures in CVR studies. ASL is less prone to CBV and large vessel effects, particularly in veins. However, ASL also shows nonlinearities in response to changes in $P_{ET}CO_2$, albeit in different regions of the $PaCO_2$ range than BOLD. In comparison with BOLD, ASL has about half the signal-to-noise ratio present in normal tissues. Furthermore, it is limited by transit time effects at low flows. Mayhew *et al*[9] showed that in a fMRI model, there is a very tight correlation with BOLD in healthy subjects when flow is stimulated by neuroactivation. In a study comparing BOLD CVR with ASL CVR in patients with severe cerebrovascular disease, there was an excellent correlation between the two methods.[11] In fact, the spatial extent of steal physiology was very similar for both. Another advantage of ASL is that 2 seconds temporal resolution available with BOLD is also achievable with ASL. Unfortunately, the ASL sequence used in this study was not capable of capturing the entire brain being limited

to only a few slices. It is expected that future implementations of ASL may overcome these limitations.

CONCLUSION

We introduce a method to calculate the time constant, τ, of the BOLD response to a step increase in a vasoactive stimulus, $PaCO_2$, to characterize the dynamics of cerebrovascular reactivity. We illustrate the results of this analysis in a cohort of 20 patients with known unilateral carotid artery occlusion and abnormal vascular response assessed with CVR. We found that τ was prolonged in areas downstream from high-grade carotid stenosis, while the contralateral hemisphere was consistently spared. Abnormality was assessed with *z* values relative to a site-specific atlas to make them compatible, in the future, with data from other investigators who take the same approach.

We conclude that τ, or the speed of response, and ssCVR, the steady-state magnitude of response to a stimulus, provide information about aspects of vascular reactivity that otherwise cannot be discerned from the usual measure, the CVR.

AUTHOR CONTRIBUTIONS

JP contributed to study concept and design, analysis and interpretation, writing of the manuscript. APC contributed to study concept and critical revision of the manuscript for important intellectual content. OS, KS, DMM, PD, LV, JD and DJM contributed to critical revision of the manuscript for important intellectual content. GM contributed to Figures' design and critical revision of the manuscript for important intellectual content. JAF contributed to study concept and design, writing of the manuscript, and study supervision.

DISCLOSURE/CONFLICT OF INTEREST

RespirAct is currently a noncommercial research tool assembled, and made available by Thornhill Research Inc. (TRI), a spin-off company from the University Health Network, to research institutions to enable CVR studies. JAF is the Chief Scientist and JD is the Senior Scientist at (TRI), and JP, OS, APC, DJM, and DMM have contributed to the development of RespirAct and have received payments from, or shares in, TRI.

ACKNOWLEDGMENTS

The authors thank the Toronto Western Hospital RespirActTM technologist Tien Wong, as well as the MR imaging technologists, Eugen Hlasny and Keith Ta, for their contributions to the data acquisition.

REFERENCES

1 Derdeyn CP, Videen TO, Fritsch SM, Carpenter DA, Grubb RL, Jr., Powers WJ. Compensatory mechanisms for chronic cerebral hypoperfusion in patients with carotid occlusion. *Stroke* 1999; **30**: 1019–1024.
2 Balucani C, Viticchi G, Falsetti L, Silvestrini M. Cerebral hemodynamics and cognitive performance in bilateral asymptomatic carotid stenosis. *Neurology* 2012; **79**: 1788–1795.
3 Silvestrini M, Viticchi G, Falsetti L, Balucani C, Vernieri F, Cerqua R *et al.* The role of carotid atherosclerosis in Alzheimer's disease progression. *J Alzheimers Dis* 2011; **25**: 719–726.
4 Fierstra J, Poublanc J, Han JS, Silver F, Tymianski M, Crawley AP *et al.* Steal physiology is spatially associated with cortical thinning. *J Neurol Neurosurg Psychiatry* 2010; **81**: 290–293.
5 Conklin J, Fierstra J, Crawley AP, Han JS, Poublanc J, Mandell DM *et al.* Impaired cerebrovascular reactivity with steal phenomenon is associated with increased diffusion in white matter of patients with Moyamoya disease. *Stroke* 2010; **41**: 1610–1616.
6 Silvestrini M, Vernieri F, Pasqualetti P, Matteis M, Passarelli F, Troisi E *et al.* Impaired cerebral vasoreactivity and risk of stroke in patients with asymptomatic carotid artery stenosis. *JAMA* 2000; **283**: 2122–2127.
7 Markus H, Cullinane M. Severely impaired cerebrovascular reactivity predicts stroke and TIA risk in patients with carotid artery stenosis and occlusion. *Brain* 2001; **124**: 457–467.
8 Fierstra J, Sobczyk O, Battisti-Charbonney A, Mandell DM, Poublanc J, Crawley AP *et al.* Measuring cerebrovascular reactivity: what stimulus to use? *J Physiol* 2013; **591**: 5809–5821.
9 Mayhew SD, Mullinger KJ, Bagshaw AP, Bowtell R, Francis ST. Investigating intrinsic connectivity networks using simultaneous BOLD and CBF measurements. *Neuroimage* 2014; **99**: 111–121.
10 Cohen ER, Ugurbil K, Kim SG. Effect of basal conditions on the magnitude and dynamics of the blood oxygenation level-dependent fMRI response. *J Cereb Blood Flow Metab* 2002; **22**: 1042–1053.
11 Mandell DM, Han JS, Poublanc J, Crawley AP, Fierstra J, Tymianski M *et al.* Quantitative measurement of cerebrovascular reactivity by blood oxygen level-dependent MR imaging in patients with intracranial stenosis: preoperative cerebrovascular reactivity predicts the effect of extracranial-intracranial bypass surgery. *AJNR Am J Neuroradiol* 2011; **32**: 721–727.
12 Regan RE, Fisher JA, Duffin J. Factors affecting the determination of cerebrovascular reactivity. *Brain Behav* 2014; **4**: 775–788.
13 Regan RE, Duffin J, Fisher JA. Instability of the middle cerebral artery blood flow in response to CO_2. *PLoS One* 2013; **8**: e70751.
14 Thomas BP, Liu P, Park DC, van Osch MJ, Lu H. Cerebrovascular reactivity in the brain white matter: magnitude, temporal characteristics, and age effects. *J Cereb Blood Flow Metab* 2014; **34**: 242–247.
15 Vazquez AL, Cohen ER, Gulani V, Hernandez-Garcia L, Zheng Y, Lee GR *et al.* Vascular dynamics and BOLD fMRI: CBF level effects and analysis considerations. *Neuroimage* 2006; **32**: 1642–1655.
16 Cantin S, Villien M, Moreaud O, Tropres I, Keignart S, Chipon E *et al.* Impaired cerebral vasoreactivity to CO2 in Alzheimer's disease using BOLD fMRI. *Neuroimage* 2011; **58**: 579–587.
17 Sobczyk O, Battisti-Charbonney A, Fierstra J, Mandell DM, Poublanc J, Crawley AP *et al.* A conceptual model for CO-induced redistribution of cerebral blood flow with experimental confirmation using BOLD MRI. *Neuroimage* 2014; **92**: 56–68.
18 van der Zande FH, Hofman PA, Backes WH. Mapping hypercapnia-induced cerebrovascular reactivity using BOLD MRI. *Neuroradiology* 2005; **47**: 114–120.
19 Mark CI, Slessarev M, Ito S, Han J, Fisher JA, Pike GB. Precise control of end-tidal carbon dioxide and oxygen improves BOLD and ASL cerebrovascular reactivity measures. *Magn Reson Med* 2010; **64**: 749–756.
20 St Croix CM, Cunningham DA, Kowalchuk JM, McConnell AK, Kirby AS, Scheuermann BW *et al.* Estimation of arterial PCO_2 in the elderly. *J Appl Physiol* 1995; **79**: 2086–2093.
21 Jones NL, Campbell EJ, Edwards RH, Wilkoff WG. Alveolar-to-blood PCO_2 difference during rebreathing in exercise. *J Appl Physiol* 1969; **27**: 356–360.
22 Spano VR, Mandell DM, Poublanc J, Sam K, Battisti-Charbonney A, Pucci O *et al.* CO_2 blood oxygen level-dependent MR mapping of cerebrovascular reserve in a clinical population: safety, tolerability, and technical feasibility. *Radiology* 2013; **266**: 592–598.
23 Sobczyk O, Battisti-Charbonney A, Poublanc J, Crawley AP, Sam K, Fierstra J *et al.* Assessing cerebrovascular reactivity abnormality by comparison to a reference atlas. *J Cereb Blood Flow Metab* 2015; **35**: 213–220.
24 Slessarev M, Han J, Mardimae A, Prisman E, Preiss D, Volgyesi G *et al.* Prospective targeting and control of end-tidal CO_2 and O_2 concentrations. *J Physiol* 2007; **581**: 1207–1219.
25 Brogan TV, Robertson HT, Lamm WJ, Souders JE, Swenson ER. Carbon dioxide added late in inspiration reduces ventilation-perfusion heterogeneity without causing respiratory acidosis. *J Appl Physiol* 2004; **96**: 1894–1898.
26 Ito S, Mardimae A, Han J, Duffin J, Wells G, Fedorko L *et al.* Non-invasive prospective targeting of arterial P(CO2) in subjects at rest. *J Physiol* 2008; **586**: 3675–3682.
27 Ashburner J, Friston K. Multimodal image coregistration and partitioning—a unified framework. *Neuroimage* 1997; **6**: 209–217.
28 Poublanc J, Han JS, Mandell DM, Conklin J, Stainsby JA, Fisher JA *et al.* Vascular steal explains early paradoxical blood oxygen level-dependent cerebrovascular response in brain regions with delayed arterial transit times. *Cerebrovasc Dis Extra* 2013; **3**: 55–64.
29 Richiardi J, Monsch AU, Haas T, Barkhof F, Van de Ville D, Radu EW *et al.* Altered cerebrovascular reactivity velocity in mild cognitive impairment and Alzheimer's disease. *Neurobiol Aging* 2014; **36**: 33–41.
30 Minoshima S, Frey KA, Koeppe RA, Foster NL, Kuhl DE. A diagnostic approach in Alzheimer's disease using three-dimensional stereotactic surface projections of fluorine-18-FDG PET. *J Nucl Med* 1995; **36**: 1238–1248.
31 Chetelat G, Desgranges B, Landeau B, Mezenge F, Poline JB, de la Sayette V *et al.* Direct voxel-based comparison between grey matter hypometabolism and atrophy in Alzheimer's disease. *Brain* 2008; **131**: 60–71.
32 Berry CB, Myles PS. Preoxygenation in healthy volunteers: a graph of oxygen 'washin' using end-tidal oxygraphy. *Br J Anaesth* 1994; **72**: 116–118.
33 Gilden D, Cohrs RJ, Mahalingam R, Nagel MA. Varicella zoster virus vasculopathies: diverse clinical manifestations, laboratory features, pathogenesis, and treatment. *Lancet Neurol* 2009; **8**: 731–740.

34 McColl BW, Allan SM, Rothwell NJ. Systemic infection, inflammation and acute ischemic stroke. *Neuroscience* 2009; **158**: 1049–1061.
35 Han JS, Mandell DM, Poublanc J, Mardimae A, Slessarev M, Jaigobin C *et al.* BOLD-MRI cerebrovascular reactivity findings in cocaine-induced cerebral vasculitis. *Nat Clin Pract Neurol* 2008; **4**: 628–632.
36 Muller A, Remmele S, Wenningmann I, Clusmann H, Traber F, Flacke S *et al.* Analysing the response in R2* relaxation rate of intracranial tumours to hyperoxic and hypercapnic respiratory challenges: initial results. *Eur Radiol* 2011; **21**: 786–798.
37 Mutch WA, Ellis MJ, Graham MR, Wourms V, Raban R, Fisher JA *et al.* CO_2 stress testing: a pilot study in patients with concussion. *PLoS One* 2014; **9**: e102181.
38 Davis TL, Kwong KK, Weisskoff RM, Rosen BR. Calibrated functional MRI: mapping the dynamics of oxidative metabolism. *Proce Natl Acad Sci* 1998; **95**: 1834–1839.
39 Hoge RD, Atkinson J, Gill B, Crelier GR, Marrett S, Pike GB. Investigation of BOLD signal dependence on cerebral blood flow and oxygen consumption: the deoxyhemoglobin dilution model. *Magn Reson Med* 1999; **42**: 849–863.
40 Halani S, Kwinta JB, Golestani AM, Khatamian YB, Chen JJ. Comparing cerebrovascular reactivity measured using BOLD and cerebral blood flow MRI: The effect of basal vascular tension on vasodilatory and vasoconstrictive reactivity. *Neuroimage* 2015; **110**: 110–123.
41 Bulte DP, Chiarelli PA, Wise RG, Jezzard P. Cerebral perfusion response to hyperoxia. *J Cereb Blood Flow Metab* 2007; **27**: 69–75.
42 Prisman E, Slessarev M, Han J, Poublanc J, Mardimae A, Crawley A *et al.* Comparison of the effects of independently-controlled end-tidal PCO(2) and PO(2) on blood oxygen level-dependent (BOLD) MRI. *J Magn Reson Imaging* 2007; **27**: 185–91.
43 Battisti-Charbonney A, Fisher J, Duffin J. The cerebrovascular response to carbon dioxide in humans. *J Physiol* 2011; **589**: 3039–3048.
44 Alderliesten T, De Vis JB, Lemmers PM, van Bel BF, Benders MJ, Hendrikse J *et al.* Simultaneous quantitative assessment of cerebral physiology using respiratory-calibrated MRI and near-infrared spectroscopy in healthy adults. *Neuroimage* 2013; **85**: 255–263.
45 Yezhuvath US, Lewis-Amezcua K, Varghese R, Xiao G, Lu H. On the assessment of cerebrovascular reactivity using hypercapnia BOLD MRI. *NMR Biomed* 2009; **22**: 779–786.
46 Yablonskiy DA. Cerebral metabolic rate in hypercapnia: controversy continues. *J Cereb Blood Flow Metab* 2011; **31**: 1502–1503.

Supplementary Information accompanies the paper on the Journal of Cerebral Blood Flow & Metabolism website (http://www.nature.com/jcbfm)